NJC

Accepted Manuscript

This is an *Accepted Manuscript*, which has been through the Royal Society of Chemistry peer review process and has been accepted for publication.

Accepted Manuscripts are published online shortly after acceptance, before technical editing, formatting and proof reading. Using this free service, authors can make their results available to the community, in citable form, before we publish the edited article. We will replace this *Accepted Manuscript* with the edited and formatted *Advance Article* as soon as it is available.

You can find more information about *Accepted Manuscripts* in the Information for Authors.

Please note that technical editing may introduce minor changes to the text and/or graphics, which may alter content. The journal's standard Terms & Conditions and the Ethical guidelines still apply. In no event shall the Royal Society of Chemistry be held responsible for any errors or omissions in this *Accepted Manuscript* or any consequences arising from the use of any information it contains.

ROYAL SOCIETY OF CHEMISTRY

www.rsc.org/njc

Journal Name

ARTICLE

Control the Morphology of Calcium Sulfate Hemihydrate Using Aluminum Chloride as Habit Modifier

Received 00th January 20xx,
Accepted 00th January 20xx

DOI: 10.1039/x0xx00000x

www.rsc.org/

Wenpeng Zhao, Chuanhui Gao , Guangyu Zhang, Jun Xu, Chuanxing Wang , Yumin Wu

Abstract: The morphology and aspect ratio of calcium sulfate hemihydrate (HH) are successfully controlled using $AlCl_3$ as morphology modifier in the hydrothermal synthesis process. As the concentration of $AlCl_3$ is increased from 0 to 7.5 × 10−2 mol·L^{-1}, the crystal length decreases from 130 μm to 0.1-0.3 μm and the corresponding aspect ratio declined dramatically from 150-240 to 1-2, and the crystal morphology gradually changes from whisker to rod, and even irregular nanogranules. The preferential adsorption of Al^{3+} on the side facets of HH would lower the surface energy inhibited the elongation along these facets. The doping of Al^{3+} in the HH would distroyed the main chain of HH inhibited the elongation along [001] direction. The two facts contribute to the morphology control. The work exhibits an efficient method to controlling the morphology of HH over a large range of size by simply adjusting the concentration of $AlCl_3$.

1. Introduction

Synthesis of nano-sized and micrometer-sized material with controllable morphology has attracted increasingly interest in materials chemistry due to morphology-dependent optical electronic, magnetic, catalytic, and biomedical properties [1-4]. Numerous researches have focused on preparing materials with multifarious morphologies, such as wires, rods, tubes, disks, and hollow particles [5-9].

The performance of calcium sulfate hemihydrate (HH) in different applications is strongly related to the morphology and size of crystal. HH crystals with low aspect ratio, exhibiting superior mechanical properties and good flowability, are suitable for using as bone cement [10]. HH crystals with high aspect ratios, including whiskers and wires, are widely used in plastics, ceramics, rubber, paper making as reinforcing materials, owing to their superior thermal stability, chemical resistance and excellent compatibility [11, 12]. Recently, some researchers synthesized nano-sized HH crystals used as drug carrier, an important emerging application of HH, which further extends the application area of HH [13, 14]. Therefore, controlling the morphology of HH is very important to achieving the expected properties to satisfy the practical application.

The morphology of HH crystals can be controlled by lots of strategies, including changing pH of the solution, microwave-assisted method, the use of crystal shape modifiers and reverse micellar method. For instance, as the pH increased from 1.5 to 8.78, the aspect ratio of HH crystal reduced from 9.04 to 1.23 [15]; HH crystal nanowires with aspect ratio up to 62 was synthesized by microwave-assisted method [16]; the presence of glycerol, Mg^{2+} and ethanediol increased the aspect ratios of HH crystals up to 118, 370 and 400 [17-19], respectively. The aspect ratios of HH crystals increased from 1.7 to 4.8 by adding an appropriate amount of ethanol, potassium sodium tartrate and sodium citrate, respectively [20-22]. However, the aspect ratio is merely adjusted in a narrow range. The morphology of HH crystal can be controlled over a large range of size using reverse microemulsions of water, n-hexanol, cetyltrimethyl ammonium bromide (CTAB) and sodium dodecyl sulfonate (SDS) [23]. The aspect ratios can be adjusted from 2-7 to 180-250 and eventually to nanogranules. However, comparing to hydrothermal process, the process of the reverse micromemulsion method is complicated and lots of organic solvent and surfactants are used.

Herein, a simple approach was developed to controlling HH crystal morphology over a large range of size through hydrothermal treatment calcium sulphate dehydrate ($CaSO_4 \cdot H_2O$, DH, gypsum) derived from oyster shells using aluminum chloride as habit modifier. The morphology of HH crystal can be controlled over a large range of size by simply adjusted the concentration of $AlCl_3$.The adsorption and doping of Al^{3+} on/in HH crystal contribute to the morphology control, and the corresponding mechanism has been discussed.

[a] School of Chemical Engineering, Qingdao University of Science and Technology, 53 Zhengzhou Road, Qingdao 266042, (China). Email: wuyumin005@163.com

Electronic Supplementary Information (ESI) available: [Enlarged Figure 1f, EDS analysis, enlarged XRD patterns.]. See DOI: 10.1039/x0xx00000x

2. Experimental

2.1. Experiment Procedure

Commercial chemicals with analytical grade were used in the experiments. Calcium sulfate dihydrate, synthesized from oyster shells [24], mixed with deionized water and a certain amount of aluminum chloride with a purity of 99.8% at room temperature to get the suspensions containing 1.0～5.0 wt % calcium sulfate dihydrate and 0 to 7.5 × 10^{-2} mol·L^{-1} aluminum chloride. The slurries were then treated under hydrothermal condition (140 °C, 4.0～12.0 h), filtrated, and dried at 105 °C for 6.0 h.

2.2. Characterization.

The morphology of the HH crystals were characterized using the field-emission scanning electron microscopy (SEM, JEOL JSM-6, Japan), the high-resolution transmission electron microscopy (HRTEM, JEM-2100, Japan) equipped with the selected area electron diffraction (SAED). The structures of the HH crystals were identified by powder X-ray diffractometer (XRD, Rigaku D-MAX-2500/PC, Japan) using Cu *Kα1* radiation (λ=1.54178 Å), with a scanning rate of 2 $^{o}min^{-1}$ and scanning 2ϑ range of 5 to 40^{o}. X-ray photoelectron spectrometer (XPS, Thermo ESCALAB 250Xi, USA) was employed to examine the surface adsorption of aluminium chloride by using an Al Kα X-ray source operated at 150W.The adsorption style between Al^{3+} and SO_4^{2-} was investigated by attenuated total reflectance Fourier transform infrared spectroscopy (ATR-FTIR, Vertex 70, USA). The average diameters and the lengths of the whiskers for each sample were estimated by direct measuring about 100 whiskers from the typical optical micrographs with the magnifications of 100-1000.

3. Results and discussion

3.1. Morphology control of HH crystals

According to the theoretical fundamentals of crystal growth, the final external shape of a crystal depends on the relative growth rates of different crystal faces, which could be changed by modifying thermodynamic and/or kinetic parameters of the crystallization environment [25]. Some additive agents called crystal shape modifier have been added, in order to controlling the morphology of HH crystals. HH crystals were synthesized by hydrothermal method in the presence of various concentrations of $AlCl_3$ whereas other experimental conditions were fixed. The SEM images of HH crystals are shown in Figure 1. HH crystals with an average length of 123 μm, an average width of 0.93 μm were synthesized in the absence of $AlCl_3$ (shown in Figure 1a). When the concentration of $AlCl_3$ was 2.5×10^{-3} mol·L^{-1}, the crystals were significantly elongate along the [001] direction with the length up to 132 μm while the mean width declined to 0.6 μm (shown in Figure 1b). Further increasing the $AlCl_3$ concentration to 2.5× 10^{-2} mol·L^{-1} let to forming short rods with 3.0-7.0 μm in length and 0.2-0.5 μm in width (shown in Figure 1c). Increasing the concentration of $AlCl_3$ to 7.5×10^{-2} mol·L^{-1} led to forming HH crystals of about 100-300 nm, in the form of irregular nanogranules (shown in Figure 1d). The data indicate that the HH crystal length along the *c axis* and the corresponding width are strongly dependent on the concentration of $AlCl_3$. TEM, SAED, and high resolution electron microscopy (HRTEM) were carried out to further study the morphology and structure of HH crystal. Figure 1e exhibits the HH crystal in the form of long rod, and the SAED pattern shows that near the (000) plane (insert image shown in Figure 1f, the enlarged Figure 1f shown in supporting information) were identified as (114), (112), and (006), taken from the [1$\bar{1}$0] zone axis; they matched the vector relationship of crystal planes. According to the SAED pattern, we confirm that the HH crystals are single crystals grown [001] direction. Figure 1e, f exhibited that the distance of the lattice fringes along the elongation of the crystal was 0.5963 nm, quite similar to the d_{002}=0.599 nm of HH, further confirming the HH crystals grown [001] direction.

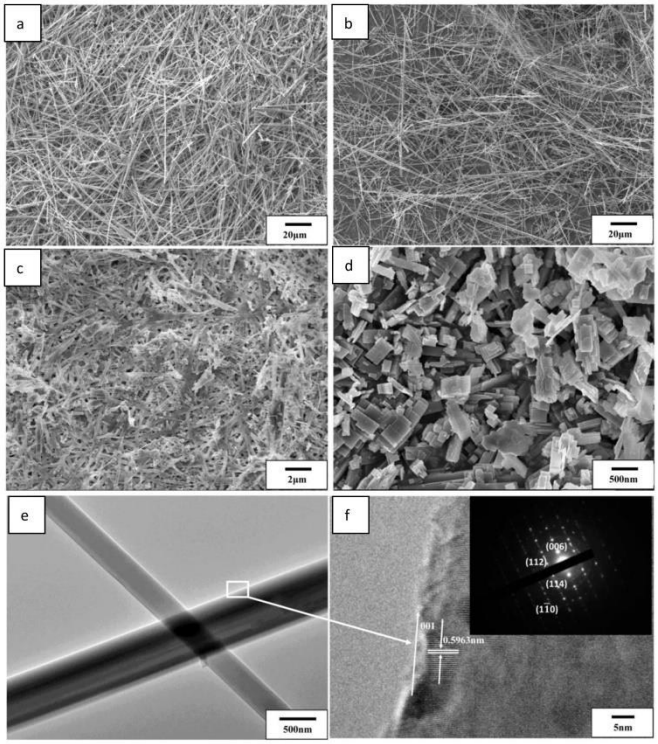

Figure 1 SEM images of HH crystal synthesized at the concentration of $AlCl_3$ (mol·L^{-1}): (a) 0, (b) 2.5× 10^{-3}, (c) 2.5× 10^{-2} (d) 7.5× 10^{-2}.(e, f) TEM and HRTEM images and SAED pattern of HH crystal in the presence of 2.5× 10^{-3} mol·L^{-1} $AlCl_3$

Aspect ratio is defined as the ratio of the length of the *c axis* to that of *a axis*. As shown in Figure 2, the aspect ratio of HH crystals is changing over a wide range. Increasing the concentration of $AlCl_3$ from 2.5×10^{-3} to 7.5×10^{-2} mol·L^{-1} results in the aspect ratio decreasing from 150-240 to 1-2. Thus, the $AlCl_3$ assistant method offers an approach to control the morphology and size of HH crystals over a wide range by simply changing the concentration of $AlCl_3$.

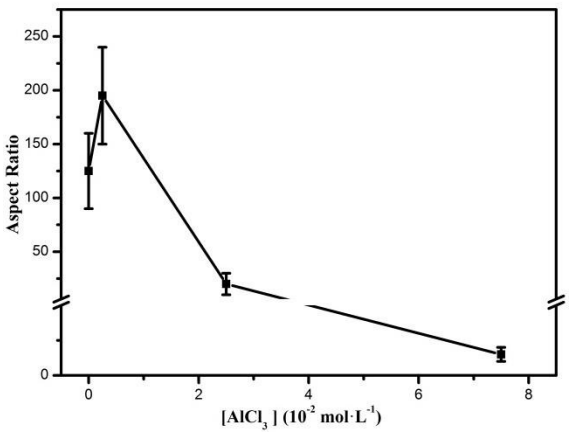

Figure 2 Aspect ratio of HH crystal as a function of the concentration of $AlCl_3$

3.2. Growth mechanism of HH crystal in the presence of $AlCl_3$

Energy dispersive spectrometry (EDS) analysis was used to confirm the present of Al on the surface of HH crystal (Supporting information Figure S2). The atomic percent of Al was increased with the increase in concentration of $AlCl_3$, while the atomic ratios of Ca/S were decreased. These results indicated that Al was absorbed on the surface of HH crystal. The preferential adsorption of Al^{3+} on the HH crystal is responsible for the controllable morphology.

The preferential adsorption of Al^{3+} on the surfaces of HH crystal can be associated with the structure of HH crystal. The crystal lattice of HH is compose of repeating unit, Ca and SO_4 atoms ionically bonded in the form of -SO_4–Ca-SO_4-Ca-SO_4- in which every S atom is covalently bonded with four O atoms forming a tetrahedral structure [26, 27]. These hexagonally arranged chains form a framework along [001] direction with consecutive channels with a diameter of about 4.5Å, where every two calcium sulfate molecules share one water molecule [28]. Thus, SO_4^{2-} ions present a denser distribution on the side facets of [110], and [100], and Ca^{2+} ions present a denser distribution on the top facet of [001] [23]. Thus, the Al^{3+} ions with positive charge are easier to adsorb on the side facets than on the top facet.

On the basis of the fact that Al^{3+} is adsorbed on the surface of HH crystals that was negatively charged, the detail adsorption style of Al^{3+} is investigated using ATR-FTIR spectroscopy. As shown in Figure 3 curve a, the peak located at 1007 cm^{-1} is ascribed to the distorted symmetric stretching of υ1 band of SO_4^{2-}, the triple peaks located at 1150, 1129, and 1085 cm^{-1} are related to the active υ3 band of SO_4^{2-}. The presence of four bands in the υ S-O stretching region indicated that the adsorbed sulfate has C2υ symmetry and the sulfate is bonded to the metal ion through two oxygens in the form of –Me-O-S(O_2)-O-Me- named bidentate binuclear [29]. This related to the main chain, -SO_4–Ca-SO_4-Ca-SO_4-, of HH crystal. Compared to curve a, the peak at 1150 and 1129 cm^{-1} shifted to 1140 and 1110 cm^{-1} in curve b, c, and d, respectively. This indicated the sulfate is bonded to the metal ion through two oxygens in the form of –Me-(O_2) -S(O_2) named bidentate mononuclear [30-32]. This may be attributed to the adsorption of Al^{3+} on the surface of HH crystals in the form of –Al-(O_2) -S(O_2).

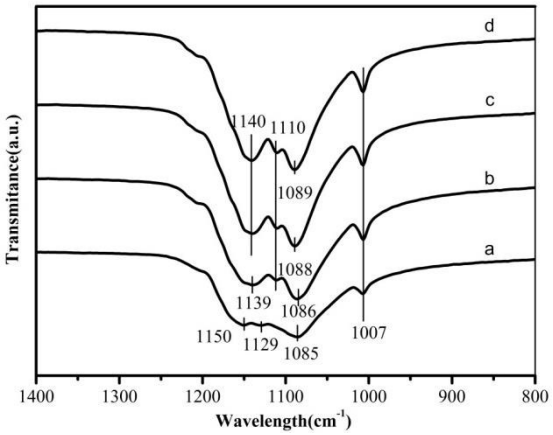

Figure 3 ATR-FTIR spectra of HH crystals formed in the presence of $AlCl_3$(mol·L^{-1}): (a) 0, (b) 2.5× 10^{-3}, (c) 2.5× 10^{-2} , (d) 7.5× 10^{-2}.

The XPS is employed to further confirm the adsorption styles Al^{3+} on the HH crystals. Figure 4I shows the Al 2p spectra of HH crystals, the Al 2p peaks occur in the curve b, c and d, indicating the adsorption of Al^{3+} on the HH crystals surface. As shown in Figure 4II, a single S 2p peak occurs at the binding energy of 169.27 eV in curve a, while double S 2p peaks occur in curve b, c, and d: one is located at 169.27 eV, which indicates the interaction between Ca^{2+} and SO_4^{2-} [18], and the other is located at 170.02 eV, which should be attributed to the interaction between Al^{3+} and SO_4^{2-}[33]. This confirms the adsorption of Al^{3+} on the surface of HH crystals in the form of –Al-(O_2) -S(O_2).

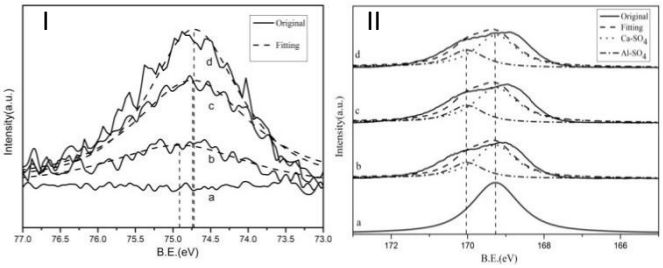

Figure 4 The XPS spectra of HH crystals formed in the present of $AlCl_3$ (mol·L^{-1}): (a) 0, (b) 2.5× 10^{-3}, (c) 2.5× 10^{-2} , (d) 7.5× 10^{-2}. (I) Al 2p peaks, and (II) S 2p peaks.

On the basis of these XPS results, the O 1s, Ca 2p, C 1s, S 2p, and Al 2p peak areas were determined. The peak areas and use of atomic sensitivity factors provide the atomic concentration of each element. The concentration values given in Table 1 were based on this [34]. Compared with the blank experiment, 1.02%, 2.13%, and 2.94% of Al were detected in the presence of 2.5× 10^{-3} , 2.5× 10^{-2}, 7.5× 10^{-2} mol·L^{-1} $AlCl_3$, respectively.

Table 1 Surface Composition of HH Crystals Detected by XPS

$AlCl_3$ (mol·L^{-1})	Ca (%)	Al (%)	S (%)	O(%)	C (%)
0	11.59	0	13.32	57.92	17.17
2.5× 10^{-3}	10.62	1.02	12.5	55.59	20.26
2.5× 10^{-2}	11.07	2.13	14.26	58.23	14.26
7.5× 10^{-2}	9.93	2.94	13.36	58.39	15.38

The preferential adsorption of Al^{3+} on the (100), and (110) facets with negative charges of HH crystals will lower the surface free energy of these facets inhibited the elongation along these facets. The crystals will then tend to grow to minimize the surface area covered by (001) facet, resulting in longer and thinner crystals (shown in Figure 1b). In addition to the surface free energy, other factors may also be at play because the surface free energy argument cannot explain the decreasing aspect ratio of crystal with increasing concentration of $AlCl_3$, when the concentration of $AlCl_3$ is greater than 2.5× 10^{-3} mol·L^{-1}. We deduce that the doping of Al^{3+} in the HH crystal is responsible for the decreasing aspect ratio of HH crystal. The -SO_4–Ca-SO_4-Ca-SO_4- chain is destroyed by Al^{3+} and a new chain, -SO_4-Ca-SO_4-Ca-SO_4-Al-SO_4, is formed. This inhibits the elongation along *c axis*, and lowers the aspect ratio.

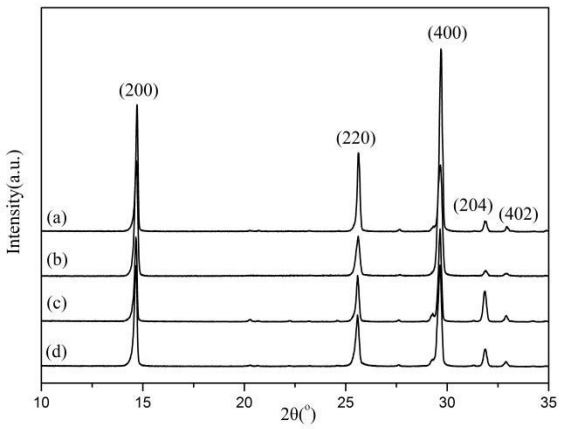

Figure 5 XRD patterns of HH crystal in the present of $AlCl_3$ (mol·L^{-1}): (a) 0, (b) 2.5× 10^{-3}, (c) 2.5× 10^{-2} (d) 7.5× 10^{-2}

Figure 5 shows the XRD patterns of HH crystal synthesized by ACl_3-assitent hydrothermal method. All of the XRD peaks were attributed to the sole existence of HH crystal. The enlarged figures of (200), (220), and (400) facets and the corresponding diffraction angle and interplanar spacing were shown in Figure s3 and Table s1. The diffraction angles of (200), (220), and (400) facets were decreased as the increase concentration of $AlCl_3$, while the interplanar spacing were increasing. The results indicated that the possible doping of Al^{3+} in the HH crystal. The doping of Al^{3+} will destroy the main chain of HH and inhibit the elongation along [001] leading to lower the aspect ratios.

As the Al 2p peaks shown in Figure 4l curve b, c and d, the peaks were located at 74.91 eV, 74.74 eV , and 74.72 eV in the presence of 2.5× 10^{-3}, 2.5× 10^{-2}, and 7.5× 10^{-2} mol·L^{-1} $AlCl_3$, respectively. The Al 2p peak at 74.91 eV was related to $Al_2(SO_4)_3$ [33], indicated that ionically bonded Al and SO_4 atoms on the surface of HH crystals. Compared with Al 2p binding energy of curve b, the Al 2p binding energies of curve c and d have shifted to the lower-energy direction, and their deviants were 0.17 and 0.19 eV, indicated that probably altered the chemical environment of Al atoms and changed the electron density of valence shell [35]. Thus, it could be supposedly attributed to the doping of Al^{3+} in the HH crystals in the form of -SO_4-Ca-SO_4-Al-SO_4. The electronegativity of Ca (1.00) is weaker than Al (1.61), which led to the shift of Al 2p peak to the smaller value than $Al_2(SO_4)_3$ [36]. Based on this, we deduce that Al^{3+} mainly adsorbs on the surface of HH crystals inhibited the radical growth of crystals, and promoted the 1-D growth of HH crystals along c axis in the presence of 2.5× 10^{-3} mol·L^{-1} $AlCl_3$. As the concentration of Al^{3+} increases to 2.5× 10^{-2}, and 7.5× 10^{-2} mol·L^{-1}, the doping of Al^{3+} in the main chains of HH crystals is occurred. This inhibits the elongation along *c axis*, and lowers the aspect ratios.

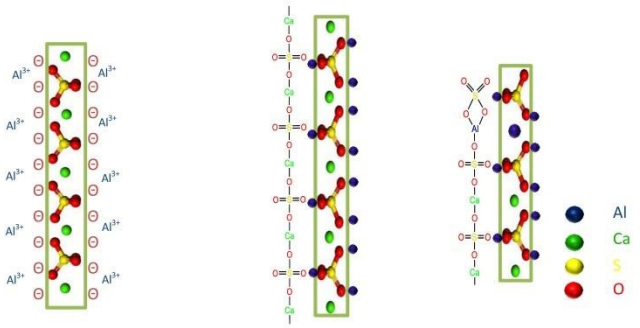

Figure 6 Schematic representation of HH crystals growth in the presence of Al^{3+}

Figure 6 shows the schematic drawing of the mechanism of HH crystals morphological changes. The [100], and [110] facets of HH crystal are negatively charged. When $AlCl_3$ is added in the hydrothermal process, Al^{3+} is expected to adsorb on these facet. This will lower the free energy on these facets and inhibit the elongation along these facets leading to longer and thinner crystal. However, while the $AlCl_3$ concentration is increasing, the doping of Al^{3+}in HH crystal would occur. This will destroy the main chain of HH crystal and inhibit the elongation along [001] direction leading to shorter crystal, ultimately resulting in a morphological transition to short rod and even irregular nanogranules with the concentration of $AlCl_3$ increasing.

4. Conclusions

The morphology and aspect ratio of HH crystal were successfully controlled over a large range of size by adjusting the $AlCl_3$ concentration in the hydrothermal process. The aspect ratio of HH crystals can be adjusted from 150-240 to 1-2. With increase in the concentration of $AlCl_3$, the morphology of HH crystal is gradually changed from whisk to short rod, and even irregular nanogranules. The controlling morphology is

attributed to the preferential adsorption of Al^{3+} on [100], and [110] facet of the HH crystals and the doping of Al^{3+} in the crystal which destroys the main chain of it. This work offers a simple approach to preparing HH crystals with various morphologies and sizes for its multiple applications.

Acknowledgements

This work is supported by the National Natural Science Foundation of China (21106075 and 21306094), Promotive research fund for excellent young and middle-aged scientists of Shandong Province (BS2012CL016), and Natural Science Foundation of Shandong Province (ZR2011BM006).

Notes and references

1 Spano, F.; Massaro, A.; Blasi, L.; Malerba, M.; Cingolani, R.; Athanassiou, A. *Langmuir* 2012, **28**, 3911−3917.
2 Tsaggeos, K.; Masiera, N.; Niwicka, A.; Dokorou, V.; Siskos, M. G.; Skoulika, S.; Michaelides, A. *Cryst. Growth Des.* 2012, 12, 2187−2194.
3 Cao, Y.; Galoppini, E.; Reyes, P. I.; Duan, Z.; Lu, Y. *Langmuir* 2012, **28**, 7947−7951.
4 Lu, W.; Wang, W.; Su, Y.; Li, J.; Jiang, L. *Nanotechnology* 2005, **16**, 2582−2586.
5 Jin, R.; Cao, Y.; Mirkin, C. A.; Kelly, K. L.; Schatz, G. C.; Zhang, J. G. *Science* 2001, **294**, 1901−1903.
6 Gentry, S. T.; Fredericks, S. J.; Krchnavek, R. *Langmuir* 2009, **25**, 2613−2621.
7 Salzemann, C.; Petit, C. *Langmuir* 2012, **28**, 4835−4841.
8 Grzelczak, M.; Pe´rez-Juste, J.; Mulvaney, P.; Liz-Marza´n, M.; Shape, L. *Chem. Soc. Rev.* 2008, **37**, 1783−1791.
9 Meagley, K. L.; Garcia, S. P. *Cryst. Growth Des.* 2012, **12,** 707−713.
10 Wang, P.; Lee, E.; Park, C.; Yoon, B.; Shin, D.; Kim, H. *J. Am. Ceram. Soc.* 2008, **91**, 2039−2042.
11 Xu, A.; Li, H.; Luo, K.; Xiang, L. *Res. Chem. Intermed.* 2011, **37**, 449−455.
12 Song, X.; Zhang, L.; Zhao, J.; Xu, Y.; Sun, Z.; Li, P.; Yu, J. *Cryst. Res. Technol.* 2011, **46**, 166−172.
13 Park, Y.; Dziak, R.; Genco, R.; Swihart, M.; Perinpanayagam, H. Calcium Sulfate Based Nanoparticles. US Patent 7767226B2, 2010.
14 Park, Y.; Mohan, K.; Al-Sanousi, A.; Almaghrabi, B.; Genco, R.; Swihart, M. T.; Dziak, R. *Biomed. Mater.* 2011, **6**, 1−11.
15 Li, F.; Liu, J.; Yang, G.; Pan, Z.; Ni, X.; Xu, H.; Huang, Q. *J. Cryst. Growth.* 2013, **374**, 31-36.
16 Li, L.; Zhu, Y.; Ma, M. *Materials Letters* 2008, 62, 4552-4554.
17 He, H.; Dong, F.; He, P.; Xu, L. *J Mater Sci* 2014, **49**, 1957-1963.
18 Hou, S; Wang, J; Wang, X; Chen, H; Xiang, L. Langmuir 2014, **30**(**32**), 9804-9810.
19 Zhao, W.; Wu, Y.; Xu, J.; Gao, C. *RSC Adv* 2015, 5, 50544-50548.
20 Shen, Z.; Guan, B.; Fu, H.; Yang, L. *J. Am. Ceram. Soc.* 2009, **92**, 2894−2899.
21 Pan, Z.; Lou, Y.; Yang, G.; Ni, X.; Chen, M.; Xu, H.; Miao, X.; Liu, J.; Hu, C.; Huang, Q. *Ceram. Int.* 2013, **39** (**5**), 5495−5502.
22 Pan, Z.; Yang, G.; Lou, Y.; Xue, E.; Xu, H.; Miao, X.; Liu, J.; Hu, C.; Huang, Q. *Int. J. Appl. Ceram. Technol.* 2012, **10**, E219−E225.
23 Kong, B.; Guan, B.; Yates, M. Z.; Wu, Z. *Langmuir* 2012, **28**, 14137−14142.
24 Zhao, W; Gao, C; Guo, F; Wu, Y. Res Chem Intermed. 2015.
25 Wang, Z.; Yue, W. *Inorganic Materials* 1996, **3**, 327-331.
26 Ballirano, P.; Maras, A.; Meloni, S.; Caminiti, R. *Eur. J. Mineral* 2001, **13**, 985−993.
27 Bezou, C.; Nonat, A.; Mutin, J. C. *J. Solid State Chem.* 1995, **117**, 165−176.
28 Freyer, D.; Voigt, W. *Monatsh. Chem.* 2003, **134**, 693−719.
29 Parfitt, R.; Smart, R.; *Soil Sci. Soc. Am. J.* 1978, **42**, 48-50.
30 Hug, S. *J Colloid Interface Sci* 1997, **188**, 415-422.
31 Peak, D.; Ford, R.; Sparks, D. *J Colloid Interface Sci* 1999, **218**, 289-299.
32 Lef èvre, G. *Adv Colloid Interface Sci* 2004, **107**, 109-123.
33 Arata, K. Solid Catalyst Treated with Anion XVIII. *Applied Catalysis* 1990, **59**, 197-204.
34 Moulder, J. F.; Stickle, W. F.; Sobol, P. E.; Bomben, K. D. Handbookof X-ray photoelectron spectroscopy; Perkin-Elmer Corporation: Eden Prairie, MN, 1992.
35 Lin, Y.; Wang, T.; Jin, Y. *Power Technology* 2002, **123**, 194-198.
36 Weaver, J.; Chai, Y.; Kroll, G.; Jin, C.; Ohno, T.; Haufler, R.; Guo, T.; Alford, J.; Conceicao, J.; Chibante, L. *Chem. Phys. Lett.* 1992, **190**, 460−464.

The morphology of HH is successfully controlled over a large range of size by simply adjusting the concentration of $AlCl_3$.